THE JOURNAL OF PHYSICAL CHEMISTRY C

pubs.acs.org/JPCC

Article

Structure Sensitivity of Acetophenone Reduction on Palladium-Modified Platinum Single-Crystal Electrodes

Matias A. Villalba and Marc T.M. Koper*

Cite This: J. Phys. Chem. C 2020, 124, 25884–25891

Read Online

ACCESS | Metrics & More | Article Recommendations | Supporting Information

ABSTRACT: The electrochemical reduction of acetophenone has been investigated in acidic conditions on the three low-index [namely (111), (110), and (100)] single-crystal platinum electrodes coated with an atomic monolayer of palladium. The adsorption and reactivity of some of the acetophenone derivatives, including benzene and acetone, within the same potential window have been compared in order to evaluate the individual reactivity of isolated functional groups and therefore possible reduction of byproducts. The selectivity and faradaic efficiency of the electrocatalytic hydrogenation (ECH) of acetophenone have been determined at selected potentials. The $Pd_{ML}Pt(110)$ is the most active surface for acetophenone hydrogenation with ca. 50% current efficiency; the other two facets are less active because of a self-poisoning process, the origin of which has not been fully resolved. The only product observed, on all three electrodes, is 1-phenylethanol. Benzene and acetone do not show significant reduction activity on these electrodes. Finally, we compare the activity trends of acetophenone and its derivatives toward ECH to those reported for platinum electrodes, showing that Pd is totally selective for the production of 1-phenylethanol, whereas Pt [especially Pt(100)] shows certain selectivity toward hydrogenolysis byproducts as well.

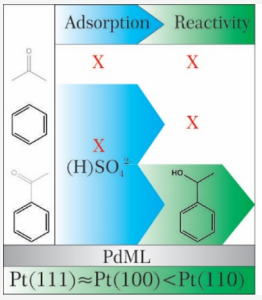

INTRODUCTION

Electrocatalytic hydrogenation (ECH) of bioderived compounds is an interesting alternative to the traditional refining of fossil-based resources, as it would in principle allow for the production of high-value fuels and chemicals entirely based on renewable building blocks and renewable electricity.[1−4] One particular case is the electroreduction of the ketone functionality, the reactivity of which is highly influenced by its chemical environment and substituents. This chemical environment will in turn modify its adsorption energy and/or the spatial orientation on the surface of different electrocatalysts,[5] and thereby its reactivity.

The simplest ketone is acetone (Ac), and its reduction has been extensively studied on platinum electrodes.[6−8] This reaction is highly structure-sensitive toward the hydrogenation product 2-propanol at Pt electrodes with (111) terraces and (110)-type steps, while the hydrogenolysis product, propane, is formed at (100)-type sites.[9] It is expected that the presence of unsaturated functional groups such as alkenes, alkynes, phenyl rings, and so forth, in the vicinity to the carbonyl group impairs the selectivity of the reduction of the ketone functionality, as these groups act as competitors for hydrogenation. A molecule such as acetophenone (AP) is a good candidate to test such effects because the phenyl ring strongly binds to Pt group surfaces,[10] and the ring can also be fully hydrogenated by transferring six protons and electrons.[11] Interestingly, it has been reported that the carbonyl group is completely reduced to ethylbenzene on polycrystalline platinum,[12] while later work on single-crystal surfaces has shown that the product distribution is facet-dependent, with again the hydrogenolysis to ethylbenzene preferentially taking place at (100) sites.[13] On the other hand, a massive palladium electrode has been employed for the same purpose, showing selectivity toward the 1-phenylethanol (PE) production, with no production of ethylbenzene.[14]

Palladium is typically considered to be the hydrogenation catalyst of choice because of the formation of a metallic hydride acting as a reducing agent. However, the structure sensitivity has never been studied on Pd electrodes primarily because of massive absorption of hydrogen in the metal lattice, deforming the catalyst and losing the atomic arrangement. One strategy to avoid hydrogen insertion is the electrodeposition of an atomic monolayer of Pd, which has previously been reported to be formed by epitaxial growth on Pt[15] single crystals. Only a very small expansion in the lattice (around 0.03 Å) compared to the Pt(111) underneath[16] has been calculated. While this does not guarantee similar chemical properties to bulk Pd, the use of a single monolayer has two main advantages: (a) it limits the diffusion of hydrogen into the bulk material[17] and thereby simplifies the electrochemical response, and (b) the shift in the d-band center is positive but very small, at least for the $Pd_{ML}Pt(111)$ surface compared to that of the Pd(111) bulk electrode,[18,19] which suggests similar electronic properties.

Received: September 15, 2020
Revised: October 30, 2020
Published: November 12, 2020

The present work studies the efficiency and selectivity of ECH of AP using three low-index Pd-type surfaces in comparison with its bare Pt substrates. The potential windows of ECH and the corresponding product distribution have been determined by voltammetry and chronoamperometry (bulk electrolysis), combined with high performance liquid chromatography (HPLC) and Fourier transform infra-red (FTIR). The ECH of AP is compared to the ECH of benzene (Bz) and Ac individually, while the competitive adsorption of the reagent and product (PE) is also tested.

EXPERIMENTAL SECTION

All the solutions were prepared using ultrapure water (Milli-Q gradient, ≥18.2 MΩ cm, TOC < 5 ppb) containing Suprapur sulfuric acid (Sigma-Aldrich) as the supporting electrolyte. The palladium precursors employed for the electrodeposition were $PdSO_4$ 98% and $PdCl_2$ 99% (Sigma-Aldrich). The organic substrates, Ac, AP, PE, and Bz were ≥99.5, 99, 98, and ≥99.9%, respectively (Merck). Deuterium oxide and deuterated perchloric acid were also provided by Merck with 99.9% and 68 wt % in D_2O, 99 atom % *D*, respectively.

The platinum single crystals were annealed before every experiment. They were either a 3 mm bead for the voltammetric experiments or a 1 cm disk for the bulk electrolysis and spectroelectrochemical experiments. A palladium monolayer was electrodeposited on Pt(111) and Pt(110) by cycling the potential, following the procedure outlined in the previous work.[15,20,21] Briefly, the potential was cycled between 0.9 and 0.06 V in a solution containing 1×10^{-4} M of $PdSO_4$ for ca. 15 cycles for Pt(111), while 2.5×10^{-6} M of $PdSO_4$ was used for Pt(110) electrodes with around 120 scans. The scan rate was 50 mV s^{-1} for both surfaces. For Pt(100), palladium deposition can also be carried out by cycling under similar conditions; however, it requires an annealing treatment using NO,[22] which is toxic and rather avoidable. A novel method was recently exploited: underpotential deposition of palladium was carried out between 0.95 and 0.8 V in an electroplating bath containing 10^{-4} M $PdCl_2$, 3×10^{-3} M HCl, and 0.1 M H_2SO_4 at 0.1 mV·s^{-1}, followed by an electro-annealing process by cycling the potential between 0.4 and 0.06 at 10 mV·s^{-1}.[23] The relevant reaction equations for the two electrodeposition methods are $Pd^{2+} + 2e^- \rightarrow Pd$ and $PdCl_4^{2-} + 2e^- \rightarrow Pd + 4\ Cl^-$, respectively.

All the experiments were conducted in Ar atmosphere after purging the solution and the headspace of the cell with Ar for at least 20 min. A platinum mesh or foil was used as the counter electrode. All potentials are measured and referred to the reversible hydrogen electrode (RHE). The glassware and Teflon o-rings/septa were cleaned in permanganate solution overnight and then boiled five times in Milli-Q water.

The voltammetric studies were performed in a typical three-electrode cell with the single-crystal working electrode in hanging meniscus configuration, using an Autolab PGSTAT12 potentiostat. Electrolysis at constant potential was performed in a H-cell divided with a Nafion proton exchange membrane. A home-made design was used, where the reference electrode was approached to the single-crystal disk using a Luggin capillary. The sampling procedure was conducted with a septa system without stopping the reaction or breaking the contact of the electrode with the solution. The reactants and products during bulk electrolysis were analyzed by an HPLC Shimadzu LC-20A system with a sample volume of 20 μL, using a Kinetex 5 μm F5 100A LC column at 45 °C and a 1-to-1 water-acetonitrile pH-adjusted mixture with sulfuric acid (0.5 mM) as the eluent.

The spectroelectrochemical experiments used a home-made cell with a Pt foil counter electrode around the working electrode, Ar inlet through the solution and headspace, and a self-contained RHE electrode. *In situ* FTIR spectroscopy experiments were performed in a Bruker Vertex 80v IR spectrophotometer in external reflection configuration using a CaF_2 prism beveled at 60°. The single-crystal electrode was pressed against the optical window creating a thin layer using a standard procedure previously reported.[24] The presented spectra correspond to an average of 200 interferograms with 4 cm^{-1} resolution using p- or s-polarized light adequately mentioned. The spectra in this work are presented as difference spectra between the working potential and a reference potential, using an Autolab PGSTAT101. Therefore, positive bands indicate consumption of solution or adsorbed species, while negative-going bands indicate generation of species or a corresponding reorientation of (adsorbed) species.

RESULTS AND DISCUSSION

Cyclic Voltammetry. Figure 1 shows the blank cyclic voltammetry of a Pd monolayer deposited on the three low-index platinum surfaces in sulfuric acid within the potential window for hydrogen underpotential adsorption (H_{UPD}) and hydrogen evolution. For all three surfaces, a more or less reversible redox couple is located at 0.22, 0.17, and 0.16 V for $Pd_{ML}Pt(111)$, $Pd_{ML}Pt(100)$, and $Pd_{ML}Pt(110)$, respectively. For the $Pd_{ML}Pt(111)$ surface, this surface redox couple corresponds to the replacement of adsorbed hydrogen by adsorbed (bi)sulfate (positive-going scan) or vice versa (negative-going scan).[22,25] For the other two surfaces, we assume an analogous process as the potential of zero charge that is just below 0.2 V for both electrodes.[21,26] In general, sulfate specific adsorption is considerably stronger on palladium surfaces compared to platinum surfaces.

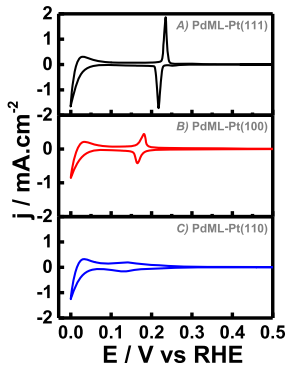

Figure 1. Cyclic voltammetry of (A) $Pd_{ML}Pt(111)$, (B) $Pd_{ML}Pt(100)$, and (C) $Pd_{ML}Pt(110)$ in pure electrolyte 0.1 M sulfuric acid at 50 mV·s^{-1}.

Figure 2 shows the cyclic voltammetry of the three electrode surfaces upon the addition of 10 mM of AP (Figure 2A–C) and 10 mM PE (Figure 2D–F).

On $Pd_{ML}Pt(111)$, a reduction wave is observed at 0.075 V in the negative-going scan with a corresponding reduction wave of lower current in the positive-going scan (Figure 2A). The charge corresponding to the reduction wave is higher than the charge for a full hydrogen monolayer in the absence of the organic molecule (ca. 587 vs 240 μC·cm^{-2}), which indicates

https://dx.doi.org/10.1021/acs.jpcc.0c08399
J. Phys. Chem. C 2020, 124, 25884−25891

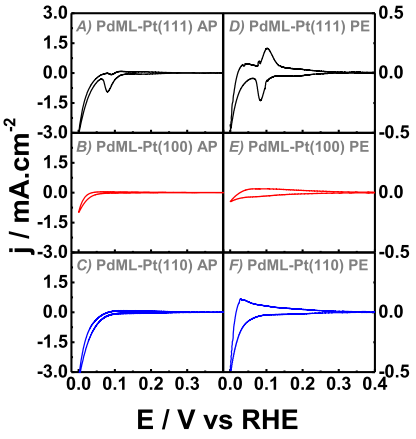

Figure 2. Cyclic voltammetry of (A,D) $Pd_{ML}Pt(111)$, (B,E) $Pd_{ML}Pt(100)$, and (C,F) $Pd_{ML}Pt(110)$ in 0.1 M sulfuric acid at 50 $mV{\cdot}s^{-1}$ in the presence of 10 mM AP and 10 mM of PE, respectively.

that AP is being reduced in this potential window, concomitantly with the reductive adsorption of hydrogen. Figure S1A shows a linear correlation between the current density and the scan rate during the negative-going scan, but its interception is negatively displaced from zero (-0.6 $mA{\cdot}cm^{-2}$). Furthermore, the current density of the wave during the positive-going scan is strongly dependent on the scan rate; a second cathodic wave appears at relatively slow scan rates. This suggests that the reduction wave in the positive-going scan also corresponds to AP reduction at relatively low scan rates, convoluted with the oxidation of adsorbed hydrogen, while at high scan rates, only re-oxidation of hydrogen is observed because of the slow kinetics of AP reduction. Additionally, the current at 0.0 V is significantly higher in the presence of AP, suggesting that at this potential, hydrogenation of the organic molecule and HER are taking place simultaneously.

In the presence of PE, which is the main expected hydrogenation product of AP,[14] the CV displays a reversible and charge-balanced redox couple at 0.09 V (Figure 2D). The potential coincides with the reduction wave in the presence of AP during the negative-going scan, although the current density is four times lower. The anodic and cathodic charges are identical (297 $\mu C{\cdot}cm^{-2}$) in the negative- and positive-going scan, and there is a linear relation between peak current and scan rate (Figure S1B), showing that the peak corresponds to a surface-adsorbed redox couple. According to the charge and the electrochemical behavior, it is likely that the signal at 0.09 V corresponds primarily to the adsorption of hydrogen with a small contribution because of anion adsorption. In contrast to the response at 0.0 V in the presence of AP, the current is greatly inhibited in the presence of PE, providing evidence that this organic molecule is not further reduced and impedes the evolution of hydrogen. We conclude that the presence of PE modifies the surface chemistry of $Pd_{ML}Pt(111)$ and that PE, in contrast to AP, is not reduced.

Sequential additions of PE to a solution containing AP, or vice versa, reveal stronger adsorption of AP compared to the alcohol. The cyclic voltammograms, as shown in Figure S2A,B, are almost identical to the one in the presence of AP alone, independently of the order of addition. These results demonstrate a stronger interaction of AP with the $Pd_{ML}Pt(111)$ surface compared to that of PE. However, based on the results discussed in the previous paragraph, we must conclude that PE can still adsorb strong enough to inhibit hydrogen evolution.

The electrochemical response of $Pd_{ML}Pt(100)$ in the presence of AP or PE is much simpler (Figure 2B,E); it causes severe suppression of voltammetric features between 0.06 and 0.4 V. The charge corresponding to the adsorption peaks (ca. 120 $\mu C{\cdot}cm^{-2}$) represents only half of the charge for hydrogen adsorption on this surface (252 $\mu C{\cdot}cm^{-2}$). The suppression in the charge indicates that the original active sites for hydrogen adsorption are hindered by the organic molecule even after the evolution of hydrogen. $Pd_{ML}Pt(100)$ does not display significant electrocatalytic activity toward the hydrogenation of AP or PE within the H_{UPD} potential region. In addition, a significantly lower current is recorded at 0.0 V when PE is present in the solution, again suggesting blockage of the surface. For both organic substrates, Figure S3 in the Supporting Information shows that the current density between 0.1 and 0.2 V scales linearly with the scan rate. This linear relation suggests the oxidation and reduction of an adsorbed species, most likely adsorbed hydrogen, which is partially blocked by the presence of the organic molecule.

Similar to $Pd_{ML}Pt(100)$, the cyclic voltammetry of $Pd_{ML}Pt(110)$ shows almost completely suppressed reduction and oxidation waves for potentials higher than 0.1 V in the presence of both AP and PE (Figure 2C,F). The current density in the potential window between 0.1 and 0.35 V shows a linear relation with the scan rate for both organic substrates, as shown in Figure S4 in the Supporting Information, confirming that these voltammetric features correspond to adsorption/desorption processes. Nevertheless, at 0.0 V, the current is increased in the presence of AP but reduced in the presence of PE, compared to the blank. This suggests that AP hydrogenation on $Pd_{ML}Pt(110)$ starts at around 0.1 V, while PE is inactive and acts as a blocking agent for H adsorption.

In order to understand the effect of the phenyl ring and the ketone moieties separately, cyclic voltammetry on all three electrodes was also performed in the presence of 10 mM of Bz or 10 mM of Ac, as shown in Figure 3A–F, respectively.

In the presence of Bz, the voltammograms are very similar compared to those obtained in the presence of PE on $Pd_{ML}Pt(111)$; a reversible couple is observed at ca. 0.09 V in

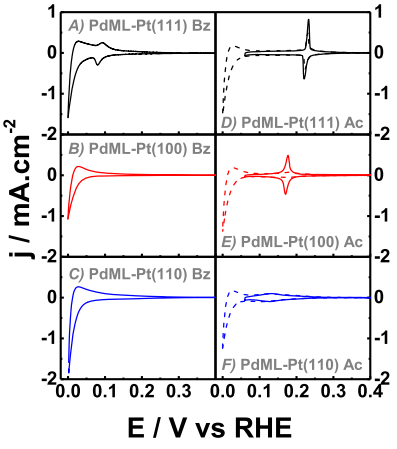

Figure 3. Cyclic voltammetry of (A,D) $Pd_{ML}Pt(111)$, (B,E) $Pd_{ML}Pt(100)$, and (C,F) $Pd_{ML}Pt(110)$ in 0.1 M sulfuric acid at 50 $mV{\cdot}s^{-1}$ in the presence of 10 mM Bz and 10 mM of Ac with solid lines, respectively. The dashed line represents addition of 100 mM of Ac.

https://dx.doi.org/10.1021/acs.jpcc.0c08399
J. Phys. Chem. C 2020, 124, 25884−25891

the H_{UPD} window with a total charge of 240 $\mu C \cdot cm^{-2}$, and the HER current at 0.0 V remains almost the same compared to the blank electrolyte. Comparing how Bz modifies the CV of Pt(111) in H_2SO_4 and HF solution[27,28] and the theoretical charge for hydrogen adsorption on Pt(111) [almost identical to Pd(111)], we propose that Bz and all the aryl derivatives studied here inhibit the adsorption of anions, while hydrogen adsorption can still take place. Taking into account similar charges resulting from the voltammetry in the presence of a weakly adsorbed anion such as perchlorate (data not shown), we conclude that anions neither affect nor participate in the ECH reaction.

Figure 3B shows that the current recorded below 0.08 V is almost identical to the blank CV on $Pd_{ML}Pt(100)$ suggesting that the phenyl ring is not hydrogenated, and HER takes place as if there is no organic substance in the solution or on the surface. A different scenario is found on $Pd_{ML}Pt(110)$ (Figure 3C), where the presence of Bz in solution increases significantly with the current at 0.0 V; this possibly indicates that the phenyl ring is being slowly reduced simultaneously to the evolution of hydrogen, as it happens on bare Pt(110).[29] Similar CV profiles were recorded by the group of Lessard and Jerkiewicz[30] on low-index Pt single-crystal surfaces within the H_{UPD} potential window, concluding that the Bz molecule hinders hydrogen and anion adsorption. On Pt electrodes, it has also been observed that Bz desorbs intact from Pt(111),[31] while on polycrystalline Pt, Bz is reduced to cyclohexane.[32]

In general, the H_{UPD} region appears more suppressed on $Pd_{ML}Pt(110)$ and $Pd_{ML}Pt(100)$ than on $Pd_{ML}Pt(111)$. This structure sensitivity matches that observed for platinum electrodes for which the adsorption enthalpies of phenol and benzaldehyde were estimated to be around 20 kJ/mol higher on (110) and (100) steps compared to (111) terraces.[33]

The presence of Ac reduces the (bi)sulfate-hydrogen exchange peaks in the blank CV of $Pd_{ML}Pt(111)$ (Figure 3D) by 30% of the charge corresponding to the forward scan. This indicates that Ac adsorbs weakly on the $Pd_{ML}Pt(111)$ electrode, but the absence of a cathodic wave or larger values of reduction charge within that potential window suggests that the Ac cannot be reduced on this surface. The current at 0.0 V remains invariant, even at higher concentrations of Ac (dashed line in Figure 3D), confirming that HER is not hindered. Conversely, the CVs for $Pd_{ML}Pt(100)$ and $Pd_{ML}Pt(110)$ electrodes in the presence of 10 mM of Ac are almost identical to their blank CVs; the H_{UPD} region remains almost the same, revealing very weak adsorption on both surfaces. Only the $Pd_{ML}Pt(100)$ electrode shows a slightly higher current in the presence 100 mM of Ac compared to the blank when the electrode is biased close to 0.0 V, suggesting Ac reduction. The trends for Ac adsorption and reduction on the palladium-coated Pt single crystals are quite different from the bare platinum electrodes. On Pt, Ac adsorbs to the Pt(110), reacts to give 2-propanol and propane on Pt(110) and Pt(100), respectively, whereas Pt(111) is the least active surface for both adsorption and hydrogenation.[9]

Quantification of the adsorbates originating from the irreversible adsorption of the phenyl compounds was performed by their electro-oxidative stripping. Figure 4 shows the cyclic voltammetry for $Pd_{ML}Pt(111)$, $Pd_{ML}Pt(100)$, and $Pd_{ML}Pt(110)$ with AP pre-adsorbed at E_{ads} = 0.5 V, then transferred to a solution free of AP, and subsequently stripped off oxidatively up to 1.5 V. This method is used employing either two cells (one for adsorption and one for stripping) or a

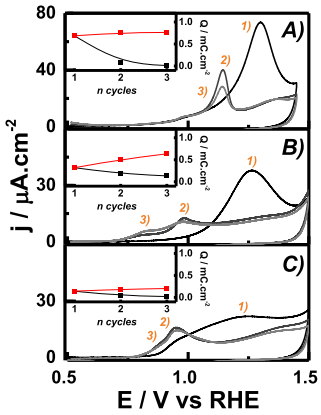

Figure 4. Anodic stripping of AP pre-adsorbed at E_{ads} = 0.5 V during the first (black), second (dark gray), and third cycle (light gray) from (A) $Pd_{ML}Pt(111)$, (B) $Pd_{ML}Pt(100)$, and (C) $Pd_{ML}Pt(110)$ in 0.1 M sulfuric acid at 10 $mV \cdot s^{-1}$. Insets show the charge estimated between 0.6 and 1.5 V for each individual cycle (black squares) and the accumulative charge (red squares).

flow cell (where the excess of aryl compounds is flushed out with the electrolyte solution), both giving similar results. The first cycle is characterized by a broad anodic wave centered at 1.3, 1.25, and 1.22 V for $Pd_{ML}Pt(111)$, $Pd_{ML}Pt(100)$, and $Pd_{ML}Pt(110)$, respectively. The second and third cycles (dark and light gray, respectively) mainly correspond to the surface oxidation of the bare substrates (Figure S5). The individual charge contributions for the second and third cycles (black squares), after background subtraction, are very small but still considered for the total accumulative oxidative charge (red squares). The accumulative oxidation charge densities for $Pd_{ML}Pt(111)$, $Pd_{ML}Pt(100)$, and $Pd_{ML}Pt(110)$ are 765, 630, and 200 $\mu C \cdot cm^{-2}$, respectively. Analogous electro-oxidation activity trends are found for PE and Bz on the Pd-decorated electrodes, while Ac does not adsorb irreversibly; hence, it is washed off during the rinsing step (see Figure S6).

The oxidation of benzoic acid was previously studied and shown to fully oxidize to CO_2 on Pt at similar potentials, giving charge density values of 353 and 328 $\mu C \cdot cm^{-2}$on Pt(110) and Pt(100), respectively, whereas on Pt(111) it is much higher, ca. 660 $\mu C \cdot cm^{-2}$.[34] The latter value agrees with the ones reported for flat-adsorbed benzoquinone[35] (considering a molecular dimension of 6-by-7 Å, very similar to Bz) and the anodic desorption charge of Bz between Pt(111) and Pt(110).[36] A discrepancy was found between the oxidative charge of Bz obtained on Pt(100), being much higher (around 1600 $\mu C \cdot cm^{-2}$), though it must be noted that for Bz, this was not a stripping charge, but a charge obtained with Bz in solution.[36]

Considering these values, and assuming that the adsorbates and their electro-oxidation residues only evolve into carbon dioxide (as it was considered for Bz,[36] toluene, benzyl alcohol,[37] and benzaldehyde[38]), we conclude that AP is irreversibly adsorbed in an essentially flat mode on $Pd_{ML}Pt(111)$ and $Pd_{ML}Pt(100)$, while the atypical low electro-oxidation charge on $Pd_{ML}Pt(110)$ might suggest (a) a lower quantity of pre-adsorbed AP or (b) a different orientation at the surface which perhaps allows only a part of the molecule to be oxidized. Density functional theory calculations[39] for Bz on Pt low-index surfaces show that interaction is dominated by van der Waals interactions, and that adsorption is the strongest on unreconstructed Pt(110). Temperature-programmed de-

https://dx.doi.org/10.1021/acs.jpcc.0c08399
J. Phys. Chem. C 2020, 124, 25884−25891

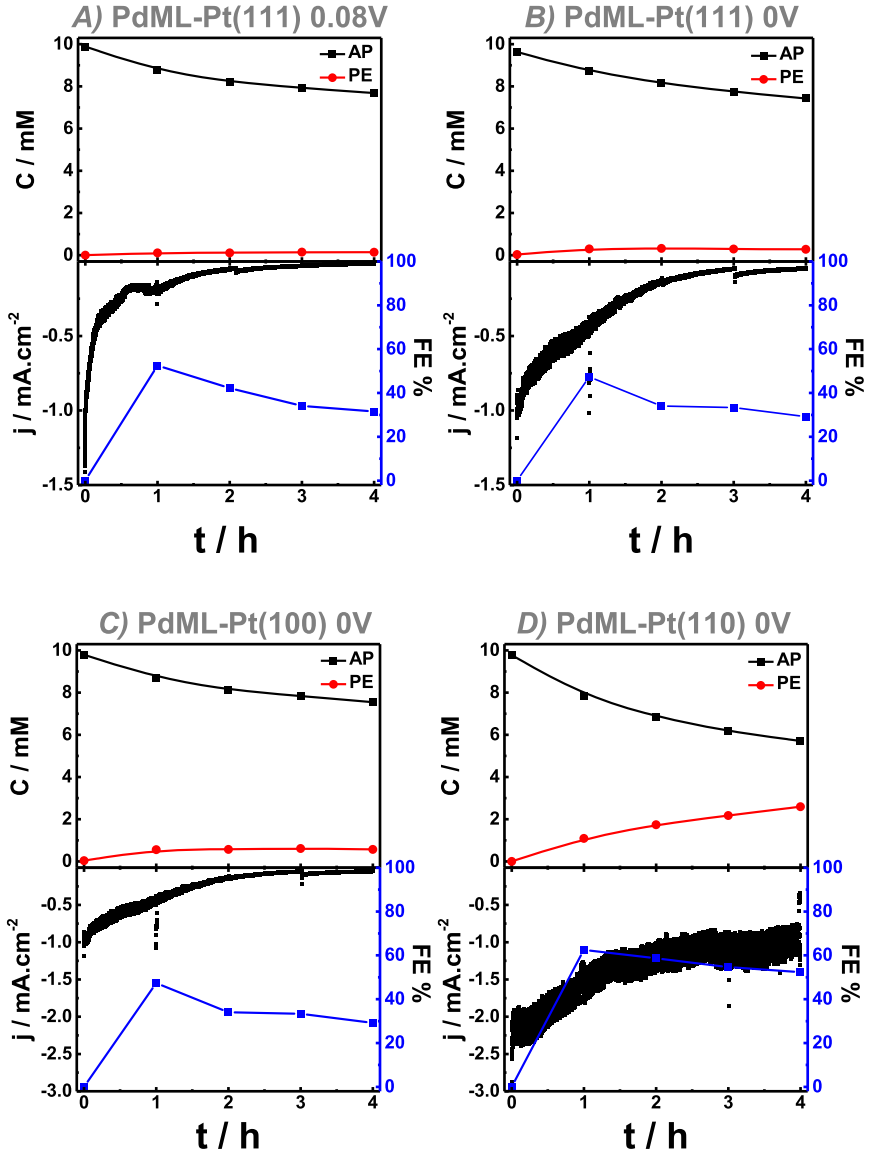

Figure 5. Evolution of current density, faradaic efficiency, and product distribution during bulk electrolysis at (A) 0.08 V on $Pd_{ML}Pt(111)$, (B) 0.0 V on the same surface, (C) 0.0 V on $Pd_{ML}Pt(100)$, and (D) 0.0 V on $Pd_{ML}Pt(110)$ with an initial AP concentration of 0.01 M in 0.1 M sulfuric acid. AP = acetophenone; PE = 1-phenylethanol.

sorption experiments in combination with NEXAFS experiments[40] indicate that on Pt(110) (1 × 2), Bz adsorbs with a nearly flat orientation with respect to the (111) microfacets of the reconstructed surface. Therefore, the low oxidation charge of AP oxidation on $Pd_{ML}Pt(110)$ remains somewhat difficult to explain.

Chronoamperometry Coupled with HPLC. Bulk electrolysis at selected potentials was performed, while the reagent and product concentrations were periodically monitored by HPLC. Figure 5 shows the compilation of the current transients and the concentration profiles for the ECH of AP on different basal planes. The Faraday efficiency was calculated as the ratio of the charge corresponding to the formation of PE to the total charge. No other product other than PE was detected. However, we note that the selectivity of the Pd_{ML} electrode cannot be unambiguously defined because there is a higher consumption of AP after 4 h of electrolysis that can be counterbalanced with the production of PE. It may be that some AP evaporation occurs during the bulk electrolysis because Ar flow is constantly passing in the headspace or that adsorption in the Nafion membrane occurred. No chemical degradation of the ketone is observed under these conditions without putting the electrode in contact with the electrolyte.

We investigated the ECH activity of the three surfaces at two different potentials: at 0.08 V, in the hydrogen underpotential deposition (H_{UPD}) region, and at 0.0 V, with simultaneous hydrogen evolution. At 0.08 V, only the $Pd_{ML}Pt(111)$ surface shows some activity (Figure 5A), in agreement with the CV results of the previous section (Figure 2A). However, the current transient shows a steep decrease within the first hour and only a small amount of PE is produced; this amount results in 32% of faradaic efficiency after 4 h of electrolysis. The very small currents and slower production of the secondary alcohol at longer electrolysis times suggest that the active sites become blocked or poisoned during the course of the reaction. A similar scenario is found when the $Pd_{ML}Pt(111)$ electrode is biased at 0.0 V (Figure 5B): the current decreases monotonically in time and reaches negligible values after 3 h, while the

https://dx.doi.org/10.1021/acs.jpcc.0c08399
J. Phys. Chem. C 2020, 124, 25884−25891

concentration of PE remains constant and below 1 mM, yielding a comparable final faradaic efficiency of ca. 30%.

The ECH activity of the $Pd_{ML}Pt(100)$ electrode at 0.0 V is similar to the $Pd_{ML}Pt(111)$ electrode in terms of current density, PE production, and faradaic efficiency (Figure 5C): the current density drops continuously within the same time scale, the alcohol formation is lower than 1 mM with a faradaic efficiency of ca. 40−50% within the first hour, levelling off at 29% after 4 h of electrolysis. In contrast, the $Pd_{ML}Pt(110)$ electrode polarized at 0.0 V (Figure 5D) offers a higher current density that drops to 50% of its initial value within the first hour but remains fairly constant for the rest of the experiment. The alcohol production increases to 2.5 mM, and the faradaic efficiency presents a maximum after the first hour but remains above 50%.

No other products such as ethylbenzene, cyclohexyl methyl ketone, or 1-cyclohexylmethanol were detected with HPLC. Ethylbenzene has been observed during AP reduction on platinum,[13] and cyclohexane has been detected at low potential for Bz hydrogenation on platinum.[31] Apparently, palladium is selective for hydrogenation of carbonyl groups over the reduction of a phenyl ring adjacent to it. The trend in the structure sensitivity for ECH reactivity at 0.0 V is (110) ≫ (100) ≈ (111) and coincides with the one found for unmodified Pt basal planes,[13] though Pt surfaces [particularly the (100) facet] also form ethylbenzene, coming from the dehydration of the ketone. The trends in activity for HER and ECH of AP on the Pd monolayers are reversed, that is, the $Pd_{ML}Pt$ (111) is the most active for HER as it is for Pt single crystals,[41] showing that the structure sensitivity of these two reactions is not linked. We note that the ECH reactivity is the highest, when the deactivation process is less pronounced [i.e., on $Pd_{ML}Pt(110)$], while the other two surfaces deactivate rapidly. Moreover, we found that the studied surfaces show no PE reduction (Figure S7), confirming its lack of reactivity within this potential window (i.e., neither dehydration of the secondary alcohol nor hydrogenation of the phenyl ring takes place).

The origin of the deactivation on $Pd_{ML}Pt(111)$ and $Pd_{ML}Pt(100)$ is still not completely understood. Figure S8 in the Supporting Information shows cyclic voltammetry of the three $Pd_{ML}(hkl)$ surfaces in 0.1 M sulfuric acid solution containing 10 mM of AP before (solid line) and after (dotted line) bulk electrolysis at 0.0 V. The current density decreased by ca 30% on the $Pd_{ML}Pt(100)$ and $Pd_{ML}Pt(110)$ electrodes, while it has reduced by around 50% on the $Pd_{ML}Pt(111)$. Adsorbed carbon monoxide (CO_{ads}) has been previously detected upon dissociative adsorption of benzaldehyde on Pt and Pd at the negative potential.[42] However, in the next section, we show using *in situ* FTIR experiments (Figure 6), the absence of C−O stretching bands from CO, which would be expected around 1920 and 2060 cm^{-1} corresponding to bridge and top positions,[43] respectively. We do note that the surface which seems to accumulate fewer adsorbates, as judged from the electro-oxidation charge, that is, $Pd_{ML}Pt(110)$ (Figure 4), is also the one that poisons the least.

***In Situ* FTIR Spectroscopy.** In order to follow the formation of adsorbates and/or the consumption/formation of species in solution upon changing the potential, FTIR experiments were conducted on all three electrodes. Figure 6 shows the spectra taken at the potentials labeled, after subtraction of the reference spectrum at 0.7 V, where no reaction occurs and the phenyl compounds show a maximum

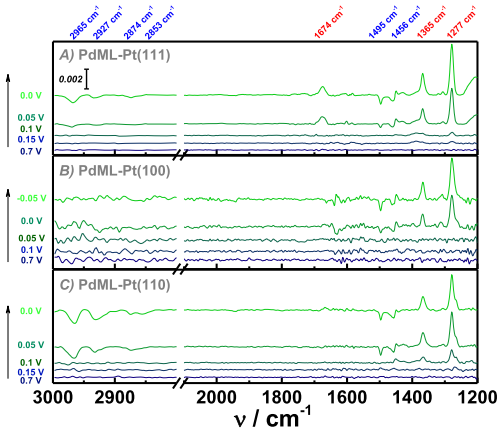

Figure 6. FTIR spectra on (A) $Pd_{ML}Pt(111)$, (B) $Pd_{ML}Pt(100)$, and (C) $Pd_{ML}Pt(110)$ at indicated potentials in a solution containing 0.01 M of AP and 0.1 M sulfuric acid under thin-film configuration.

coverage.[44] For clarity, only spectra obtained with p-polarized light are presented and spectra obtained at potentials, where no reaction takes place, were omitted. However, spectra with s-polarized light (Figure S9 in the Supporting Information) gave similar signals, and therefore, we can exclude the observation of adsorbed species. Lastly, sulfate vibrational modes are outside of the optical windows, as the CaF_2 prism strongly absorbs below 1200 cm^{-1}, precluding its observation.

On all three surfaces, two prominent and positive-pointing bands (indicated in red) located at 1365 and 1278 cm^{-1} appear below 0.2 V. They are assigned to symmetric CH_3 bending and C−C stretching between the carbonyl and the carbon of the ring,[45] respectively. A third positive-going band located at 1675 cm^{-1} appears when the potential is stepped below 0.1 V, only clearly visible for the $Pd_{ML}Pt(111)$ surface. Experiments executed in D_2O and deuterated 0.1 M perchloric acid as a supporting electrolyte (data shown in Figure S10 in the Supporting Information) show matching electrochemical signals and reveal a band at 1667 cm^{-1}, which verifies that the band at 1675 cm^{-1} in H_2O should be ascribed to a C−O carbonyl stretching wavenumber. The C−O stretching wavenumber is redshifted by ca. 8−16 cm^{-1} with respect to pure AP[45] or AP adsorbed on pristine Pt(111) in vacuum,[46] suggesting an interaction with the solvent. There are also five (possibly six) negative-going bands labeled in blue, two in the spectral region of C−C stretching in the phenyl ring (1496 and 1459 cm^{-1}) and three in the C−H stretching (2968, 2933, and 2873 cm^{-1}). These bands arise simultaneously with the disappearance of carbonyl-related band at 1278 cm^{-1} and match to the bands of the spectrum of PE in solution, as the same bands are observed for PE (as presented in Figure S11 in the Supporting Information). The consistency between the FTIR data in Figures 6 and S11 indicates that AP is only reduced to PE and that the PE desorbs when the potential is scanned negatively, but it is not further reduced.

The spectral window between 1700 and 2100 cm^{-1} does not present any bands, on any of the surfaces, showing that we can discard adsorbed CO as a possible poisoning species.

In the literature, it has been reported that Ac adsorbs through the oxygen lone electron pair.[47] However, the binding of AP to Pt(111) in the gas phase is dominated by the interaction of the phenyl ring with the surface. AP adsorbs in two different geometries on Pt(111): (a) at low coverages, the phenyl ring lies flat with the carbonyl pointing to the surface

https://dx.doi.org/10.1021/acs.jpcc.0c08399
J. Phys. Chem. C 2020, 124, 25884−25891

and the methyl group pointing away from the surface because of steric hindrance; and (b) at intermediate/high coverages, it adopts a tilted configuration with the carbonyl pointing down to the metal surface, leaving the phenyl ring and the methyl groups pointing away from the surface.[48] Interpretation of the observed IR variations can be ambiguous, but taking into account these gas-phase adsorption modes, one can envisage the following scenario. At the reference potential, the most plausible adsorption mode on the studied $Pd_{ML}Pt(111)$ surfaces is a "flat-lying" configuration with the carbonyl group pointing to the surface because the frequency of $\bar{C}O$ stretching mode slightly differs from the unperturbed stretching band. At more negative potentials, the AP is reduced to PE, which desorbs from the surface. As a result, the phenyl ring and the methyl group are becoming visible in the FTIR spectrum, because the PE is now in solution, with no preferential orientation. The desorption and weak interaction of PE with the surface could also explain the lack of reduction of the phenyl ring to produce the fully saturated ketone (cyclohexyl methyl ketone) and/or further reduction of the alcohol functionality to the corresponding alkane (ethylbenzene) via hydrogenolysis.

CONCLUSIONS

In this paper, we have studied the electrochemical hydrogenation of AP on platinum single-crystal electrodes covered by an epitaxially grown monolayer of palladium. The only product observed is PE. From our model experiments, there is no evidence for the formation of ethylbenzene, neither from further reduction of PE nor from hydrogenolysis. Moreover, no cyclohexyl methyl ketone is formed from the reduction of the phenyl ring.

$Pd_{ML}Pt(110)$ is the most active surface for AP hydrogenation at 0.0 V_{RHE} with a reasonable total Faraday efficiency of 50%. Biased at the same potential, $Pd_{ML}Pt(100)$ and $Pd_{ML}Pt(111)$ show only a small amount of PE production and suffer from a severe long-term deactivation. $Pd_{ML}Pt(111)$ is a particular case in which it is the only surface that can simultaneously adsorb hydrogen and hydrogenate AP at a potential significantly positive of the HER potential window. Unfortunately, FTIR experiments cannot detect the adsorption mode of the adsorbed organic molecules (suggesting in fact that they lie flat on the surface). The absence of adsorbed CO in the FTIR experiments indicates that CO formation is not the main reason for long-term deactivation.

All aryl derivatives, such as AP and PE, adsorb strongly on the $Pd_{ML}Pt(hkl)$ surfaces, leading to a complete blockage of anion adsorption and a partial blockage of the adsorption of hydrogen. On the other hand, Ac adsorbs very weakly on palladium and it is not reduced (not even at high concentrations ca. 100 mM).

Our results show that there are significant differences between platinum[9,13] and palladium electrodes for electrochemical hydrogenation: (a) Ac neither adsorbs nor reacts on palladium surfaces, (b) the phenyl ring in the AP molecule remains intact during the ECH, while Bz can be reduced on Pt, particularly on roughened Pt(111) and polycrystalline Pt electrodes,[31] and (c) the three low-index facets of palladium are 100% selective toward the formation of PE, whereas Pt(100) produces a detectable amount of ethylbenzene from the electroreduction of AP.[13] All the observations point toward a weaker adsorption of the molecules on the Pd monolayer system versus bare platinum electrodes.

ASSOCIATED CONTENT

Supporting Information

The Supporting Information is available free of charge at https://pubs.acs.org/doi/10.1021/acs.jpcc.0c08399.

Cyclic voltammetries, alcohol electrolysis, and FTIR spectra taken with s-polarized light, in D_2O, and in the presence of PE (PDF)

AUTHOR INFORMATION

Corresponding Author

Marc T.M. Koper − *Leiden Institute of Chemistry, Leiden University, Leiden 2300 RA, The Netherlands;* orcid.org/0000-0001-6777-4594; Email: m.koper@chem.leidenuniv.nl

Author

Matias A. Villalba − *Leiden Institute of Chemistry, Leiden University, Leiden 2300 RA, The Netherlands*

Complete contact information is available at: https://pubs.acs.org/10.1021/acs.jpcc.0c08399

Notes

The authors declare no competing financial interest.

ACKNOWLEDGMENTS

This research received funding from the Netherlands Organization for Scientific Research (NWO) in the framework of the Fund New Chemical Innovations, project 731.015.204 ELECTROGAS, with financial support of Akzo Nobel Chemicals, Shell Global Solutions, Magneto Special Anodes (an Evoqua Brand), and Elson Technologies.

REFERENCES

(1) Carneiro, J.; Nikolla, E. Electrochemical Conversion of Biomass-Based Oxygenated Compounds. *Annu. Rev. Chem. Biomol. Eng.* **2019**, *10*, 85−104.

(2) Du, L.; Shao, Y.; Sun, J.; Yin, G.; Du, C.; Wang, Y. Electrocatalytic Valorisation of Biomass Derived Chemicals. *Catal. Sci. Technol.* **2018**, *8*, 3216−3232.

(3) Kwon, Y.; Schouten, K. J. P.; van der Waal, J. C.; de Jong, E.; Koper, M. T. M. Electrocatalytic Conversion of Furanic Compounds. *ACS Catal.* **2016**, *6*, 6704−6717.

(4) Lopez-Ruiz, J. A.; Andrews, E.; Akhade, S. A.; Lee, M.-S.; Koh, K.; Sanyal, U.; Yuk, S. F.; Karkamkar, A. J.; Derewinski, M. A.; Holladay, J.; et al. Understanding the Role of Metal and Molecular Structure on the Electrocatalytic Hydrogenation of Oxygenated Organic Compounds. *ACS Catal.* **2019**, *9*, 9964−9972.

(5) Delbecq, F.; Sautet, P. Competitive C=C and C=O Adsorption of α-β-Unsaturated Aldehydes on Pt and Pd Surfaces in Relation with the Selectivity of Hydrogenation Reactions: A Theoretical Approach. *J. Catal.* **1995**, *152*, 217−236.

(6) Bänsch, B.; Härtung, T.; Baltruschat, H.; Heitbaum, J. Reduction and Oxidation of Adsorbed Acetone at Platinum Electrodes Studied by DEMS. *J. Electroanal. Chem. Interfacial Electrochem.* **1989**, *259*, 207−215.

(7) Bondue, C. J.; Koper, M. T. M. A Mechanistic Investigation on the Electrocatalytic Reduction of Aliphatic Ketones at Platinum. *J. Catal.* **2019**, *369*, 302−311.

(8) de Hemptinne, X.; Schunck, K. Electrochemical Reduction of Acetone. Electrocatalytic Activity of Platinized Platinum. *Trans. Faraday Soc.* **1969**, *65*, 591−597.

(9) Bondue, C. J.; Calle-Vallejo, F.; Figueiredo, M. C.; Koper, M. T. M. Structural Principles to Steer the Selectivity of the Electrocatalytic Reduction of Aliphatic Ketones on Platinum. *Nat. Catal.* **2019**, *2*, 243−250.

(10) Shayeghi, A.; Krähling, S.; Hörtz, P.; Johnston, R. L.; Heard, C. J.; Schäfer, R. Adsorption of Acetonitrile, Benzene, and Benzonitrile on Pt(111): Single Crystal Adsorption Calorimetry and Density Functional Theory. *J. Phys. Chem. C* **2017**, *121*, 21354−21363.
(11) Montilla, F.; Morallón, E.; Vázquez, J. L. Electrochemical Study of Benzene on Pt of Various Surface Structures in Alkaline and Acidic Solutions. *Electrochim. Acta* **2002**, *47*, 4399−4406.
(12) Pletcher, D.; Razaq, M. The Reduction of Acetophenone to Ethylbenzene at a Platinised Platinum Electrode. *Electrochim. Acta* **1981**, *26*, 819−824.
(13) Bondue, C. J.; Koper, M. T. M. Electrochemical Reduction of the Carbonyl Functional Group: The Importance of Adsorption Geometry, Molecular Structure, and Electrode Surface Structure. *J. Am. Chem. Soc.* **2019**, *141*, 12071−12078.
(14) Villalba, M.; Del Pozo, M.; Calvo, E. J. Electrocatalytic Hydrogenation of Acetophenone and Benzophenone Using Palladium Electrodes. *Electrochim. Acta* **2015**, *164*, 125−131.
(15) Inukai, J.; Ito, M. Electrodeposition Processes of Palladium and Rhodium Monolayers on Pt(111) and Pt(100) Electrodes Studied by Ir Reflection Absorption Spectroscopy. *J. Electroanal. Chem.* **1993**, *358*, 307−315.
(16) Marković, N. M.; Lucas, C. A.; Climent, V.; Stamenkovic, V.; Ross, P. N. Surface Electrochemistry on an Epitaxial Palladium Film on Pt (111): Surface Microstructure and Hydrogen Electrode Kinetics. *Surf. Sci.* **2000**, *465*, 103−114.
(17) Baldauf, M.; Kolb, D. M. A Hydrogen Adsorption and Absorption Study with Ultrathin Pd Overlayers on Au(111) and Au(100). *Electrochim. Acta* **1993**, *38*, 2145−2153.
(18) Greeley, J.; Nørskov, J. K.; Kibler, L. A.; El-Aziz, A. M.; Kolb, D. M. Hydrogen Evolution over Bimetallic Systems: Understanding the Trends. *ChemPhysChem* **2006**, *7*, 1032−1035.
(19) Kibler, L. A.; El-Aziz, A. M.; Hoyer, R. d.; Kolb, D. M. Tuning Reaction Rates by Lateral Strain in a Palladium Monolayer. *Angew. Chem., Int. Ed.* **2005**, *44*, 2080−2084.
(20) Llorca, M. J.; Feliu, J. M.; Aldaz, A.; Clavilier, J. Electrochemical Structure-Sensitive Behaviour of Irreversibly Adsorbed Palladium on Pt(100), Pt(111) and Pt(110) in an Acidic Medium. *J. Electroanal. Chem.* **1993**, *351*, 299−319.
(21) Souza-Garcia, J.; Berná, A.; Ticianelli, E. A.; Climent, V.; Feliu, J. M. Electrochemical Properties of Palladium Adlayers on Pt(110) Substrates. *J. Electroanal. Chem.* **2011**, *660*, 276−284.
(22) Chen, X.; Koper, M. T. M. Mass-Transport-Limited Oxidation of Formic Acid on a PdMLPt(100) Electrode in Perchloric Acid. *Electrochem. Commun.* **2017**, *82*, 155−158.
(23) Previdello, B. A. F.; Sibert, E.; Maret, M.; Soldo-Olivier, Y. Palladium Electrodeposition onto Pt(100): Two-Layer Underpotential Deposition. *Langmuir* **2017**, *33*, 2087−2095.
(24) Faguy, P. W.; Markovic, N.; Adzic, R. R.; Fierro, C. A.; Yeager, E. B. A Study of Bisulfate Adsorption on Pt(111) Single Crystal Electrodes Using in Situ Fourier Transform Infrared Spectroscopy. *J. Electroanal. Chem. Interfacial Electrochem.* **1990**, *289*, 245−262.
(25) Chen, X.; Granda-Marulanda, L. P.; McCrum, I. T.; Koper, M. T. M. Adsorption Processes on a Pd Monolayer-Modified Pt(111) Electrode. *Chem. Sci.* **2020**, *11*, 1703−1713.
(26) Álvarez, B.; Berná, A.; Rodes, A.; Feliu, J. M. Electrochemical Properties of Palladium Adlayers on Pt(100) Substrates. *Surf. Sci.* **2004**, *573*, 32−46.
(27) Yau, S.-L.; Kim, Y.-G.; Itaya, K. In Situ Scanning Tunneling Microscopy of Benzene Adsorbed on Rh(111) and Pt(111) in HF Solution. *J. Am. Chem. Soc.* **1996**, *118*, 7795−7803.
(28) Jerkiewicz, G.; Deblois, M.; Radovic-Hrapovic, Z.; Tessier, J.-P.; Perreault, F.; Lessard, J. Underpotential Deposition of Hydrogen on Benzene-Modified Pt(111) in Aqueous H2SO4. *Langmuir* **2005**, *21*, 3511−3520.
(29) Schmiemann, U.; Baltruschat, H. The Influence of the Single-Crystal Orientation on the Electrocatalytic Hydrogenation of Benzene and the H-D Exchange. *J. Electroanal. Chem.* **1993**, *347*, 93−109.
(30) Deblois, M.; Lessard, J.; Jerkiewicz, G. Influence of Benzene on the Hupd and Anion Adsorption on Pt(110), Pt(100) and Pt(111) Electrodes in Aqueous H2so4. *Electrochim. Acta* **2005**, *50*, 3517−3523.
(31) Hartung, T.; Schmiemann, U.; Kamphausen, I.; Baltruschat, H. Electrodesorption from Single-Crystal Electrodes: Analysis by Differential Electrochemical Mass Spectrometry. *Anal. Chem.* **1991**, *63*, 44−48.
(32) Hartung, T.; Baltruschat, H. Differential Electrochemical Mass Spectrometry Using Smooth Electrodes: Adsorption and Hydrogen/Deuterium Exchange Reactions of Benzene on Platinum. *Langmuir* **1990**, *6*, 953−957.
(33) Singh, N.; Sanyal, U.; Fulton, J. L.; Gutiérrez, O. Y.; Lercher, J. A.; Campbell, C. T. Quantifying Adsorption of Organic Molecules on Platinum in Aqueous Phase by Hydrogen Site Blocking and in Situ X-Ray Absorption Spectroscopy. *ACS Catal.* **2019**, *9*, 6869−6881.
(34) Montilla, F.; Morallón, E.; Vázquez, J. L. Electrochemical Behaviour of Benzoic Acid on Platinum and Gold Electrodes. *Langmuir* **2003**, *19*, 10241−10246.
(35) Soriaga, M. P.; Stickney, J. L.; Hubbard, A. T. Electrochemical Oxidation of Aromatic Compounds Adsorbed on Platinum Electrodes. *J. Electroanal. Chem.* **1983**, *144*, 207−215.
(36) Montilla, F.; Huerta, F.; Morallon, E.; Vazquez, J. L. Electrochemical Behaviour of Benzene on Platinum Electrodes. *Electrochim. Acta* **2000**, *45*, 4271−4277.
(37) Souto, R. M.; Rodríguez, J. L.; Pastor, E.; Iwasita, T. Spectroscopic Investigation of the Adsorbates of Benzyl Alcohol on Palladium. *Langmuir* **2000**, *16*, 8456−8462.
(38) Planes, G. A.; Moran, E.; Rodriguez, J. L.; Barbero, C.; Pastor, E. Electrochemical Behavior of Benzaldehyde on Polycrystalline Platinum. An in Situ FTIR and DEMS Study. *Langmuir* **2003**, *19*, 8899−8906.
(39) K, A. P.; Chatanathodi, R. Adsorption of Benzene on Low Index Surfaces of Platinum in the Presence of Van Der Waals Interactions. *Surf. Sci.* **2017**, *664*, 8−15.
(40) Zebisch, P.; Stichler, M.; Trischberger, P.; Weinelt, M.; Steinrück, H.-P. Tilted Adsorption of Benzene on Pt(110) 1 × 2. *Surf. Sci.* **1998**, *396*, 61−77.
(41) Marković, N. M.; Grgur, B. N.; Ross, P. N. Temperature-Dependent Hydrogen Electrochemistry on Platinum Low-Index Single-Crystal Surfaces in Acid Solutions. *J. Phys. Chem. B* **1997**, *101*, 5405−5413.
(42) Anibal, J.; Malkani, A.; Xu, B. Stability of the Ketyl Radical as a Descriptor in the Electrochemical Coupling of Benzaldehyde. *Catal. Sci. Technol.* **2020**, *10*, 3181−3194.
(43) Álvarez, B.; Rodes, A.; Pérez, J. M.; Feliu, J. M. Two-Dimensional Effects on the in Situ Infrared Spectra of Co Adsorbed at Palladium-Covered Pt(111) Electrode Surfaces. *J. Phys. Chem. B* **2003**, *107*, 2018−2028.
(44) Heiland, W.; Gileadi, E.; Bockris, J. O. M. Kinetic and Thermodynamic Aspects of the Electrosorption of Benzene on Platinum Electrodes. *J. Phys. Chem.* **1966**, *70*, 1207−1216.
(45) Chen, M.; Maeda, N.; Baiker, A.; Huang, J. Molecular Insight into Pt-Catalyzed Chemoselective Hydrogenation of an Aromatic Ketone by in Situ Modulation−Excitation Ir Spectroscopy. *ACS Catal.* **2012**, *2*, 2007−2013.
(46) Attia, S.; Schmidt, M. C.; Schröder, C.; Pessier, P.; Schauermann, S. Surface-Driven Keto−Enol Tautomerization: Atomistic Insights into Enol Formation and Stabilization Mechanisms. *Angew. Chem., Int. Ed.* **2018**, *57*, 16659−16664.
(47) Fryzuk, M. D.; Haddad, T. S.; Mylvaganam, M.; McConville, D. H.; Rettig, S. J. End-on Versus Side-on Bonding of Dinitrogen to Dinuclear Early Transition-Metal Complexes. *J. Am. Chem. Soc.* **1993**, *115*, 2782−2792.
(48) Attia, S.; Schauermann, S. Coverage-Dependent Adsorption Geometry of Acetophenone on Pt(111). *J. Phys. Chem. C* **2020**, *124*, 557−566.

https://dx.doi.org/10.1021/acs.jpcc.0c08399
J. Phys. Chem. C 2020, 124, 25884−25891